J. Min. Metall. Sect. B-Metall. 48 (3) B (2012) 383 - 390

Journal of Mining and Metallurgy, Section B: Metallurgy

THERMODYNAMIC CALCULATION OF PHASE EQUILIBRIA IN STAINLESS STEELS

G. Klančnik[a,*], D. Steiner Petrovič[b], J. Medved[a]

[a] University of Ljubljana, Faculty of Natural Sciences and Engineering, Department for Materials and Metallurgy, Ljubljana, Slovenia
[b] Institute of Metals and Technology, Ljubljana, Slovenia

(Received 19 November 2012; accepted 25 November 2012)

Abstract

In this paper two examples of thermodynamic investigation of stainless steels using both, experimental and modeling approach are described. The ferritic-austenitic duplex stainless steel and austenitic stainless steel were investigated using thermal analysis. The complex melting behavior was evident for both alloy systems. Experimentally obtained data were compared with the results of the thermodynamic calculations using the CALPHAD method. The equilibrium thermal events were also described by the calculated heat capacity. In spite of the complexity of both selected real alloy systems a relativelly good agreement was obtained between the thermodynamic calculations and experimental results.

Key words: CALPHAD, Stainless Steel, Phase diagram, Computational Thermodynamics

1. Introduction

The stainless steels are in technological sense of a great importance due to their unique properties which can be taken advantage in a wide variety of applications. The designing and optimization of stainless steels can be very time consuming and demanding due to their complex chemical composition which, among others, determines phase equilibria, mechanisms of melting, solidification, and precipitation. Nevertheless, some of the experimental methods such as thermal analyses still represents important and regular source of data in many foundries and steel plants. Using thermal analysis the liquidus and solidus can be measured, and the sequence of phase transformations, is possible to be determined.

In recent decades the research is focused in phase diagram (re)assessments. Using the CALPHAD method (CALculation of PHAse Diagrams) the phase equilibria are calculated by the relative Gibbs free energies of the phases present in particular system. One of the most important phase diagrams is the Fe-Cr-Ni ternary system, which is of main interest also in the present study.

Phase relationships in the iron-rich corner of Fe-Cr-Ni ternary system have already been intensively studied. An important experimental work on Fe-Cr-Ni system, using thermal analysis and thermodynamic modeling, was done by Kundrat and Elliott [1]. A reassessment of Cr-Fe-Ni system was also done by Hillert and Qiu [2]. Pan and Qiu [3] studied precipitation of the sigma phase in different stainless steels based on Fe-Ni-Cr ternary system where the first critical point (the precipitation of sigma phase) was determined to be at 977 °C. It was shown that it disappears with the invariant reaction in solid: $\gamma + \sigma \rightarrow \alpha + \alpha'$ at 464 °C. The α' phase represents the Cr-rich ferrite and α phase the Fe-rich ferrite. The variety of precipitates and there crystal structure in duplex and austenite stainless steels are described in references [4] and [5].

In this paper the calculations for the selected austenitic stainless steel (AISI304LN) and duplex stainless steel (SAF 2205) as relevant representatives of stainless steels were conducted. The aim of our study was to compare experimentally obtained data of real alloy systems where a ternary Fe-Cr-Ni can serve as a first approximation, with the thermodynamic calculations for binary, ternary, and multi-component systems. Using the variation of chemical composition in the performed calculations, e.g., Cr_{eq} and Ni_{eq} as a partial chemical composition, we indicate that their use should be used after critical assessment only.

2. Thermodynamic calculations

2.1 The calculation of phase equilibria

The CALPHAD [6,7] method is a semi-empirical approach used for the modeling of thermodynamic

* *Corresponding author: grega.klancnik@omm.ntf.uni-lj.si*

DOI:10.2298/JMMB121119048K

Dedicated to the memory of Professor Zbigniew Moser

properties and calculation of phase diagrams. In modeling of complex multi-component systems there is a necessity to have optimized Gibbs energy expressions of binary systems first. Additional (ternary) terms are sometimes needed, for example for ternary system where ternary compound exists and can not be predicted with the extrapolation of binaries. The predicted phase equilibria are normally very close to the optimal experimentally obtained data. For the modeling of phase equilibria a minimization of Gibbs energy is needed at given temperature, pressure and chemical composition where each phase is described with the specific thermodynamic model. Thermodynamic interaction parameters of Fe-Cr-Ni-X are listed in reference [8].

Solution phase model

The molar Gibbs energy of a substitutional solution phase, liquid phase (L), is considered as the sum of different contributions, see Eq.1. The data for pure component *i* (*i*=Fe, Cr, Ni) are taken from SGTE thermodynamic database [9]. For ternary liquid phase the Gibbs energy model is then:

$$\begin{aligned} G_m^L &= x_{Cr}\,{}^0G_{Cr}^L + x_{Fe}\,{}^0G_{Fe}^L + x_{Ni}\,{}^0G_{Ni}^L + \\ &RT(x_{Cr}\ln x_{Cr} + x_{Fe}\ln x_{Fe} + x_{Ni}\ln x_{Ni}) + x_{Cr}x_{Fe}L_{CrFe} \\ &+x_{Cr}x_{Ni}L_{CrNi} + x_{Fe}x_{Ni}L_{FeNi} + x_{Cr}x_{Fe}x_{Ni}L_{CrFeNi} \end{aligned} \quad (1)$$

Where; ${}^0G_i^L$ is the molar Gibbs free energy of pure component *i* (relative to Standard Element Reference or SER) with the phase (L), R is the gas constant, x_i mole fraction of component *i*. The excess Gibbs energy, ${}^EG_m^L$, can be expressed with the Redlich-Kister polynomials [10]:

$$L_{CrFe} = \sum_i {}^iL_{CrFe}^L (x_{Cr} - x_{Fe})^i$$

$$L_{CrNi} = \sum_i {}^iL_{CNie}^L (x_{Cr} - x_{Ni})^i$$

$$L_{FeNi} = \sum_i {}^iL_{FeNi}^L (x_{Fe} - x_{Ni})^i$$

Where ${}^iL_{Cr,Fe}^L$, ${}^iL_{Cr,Ni}^L$, ${}^iL_{Fe,Ni}^L$, are interaction parameters of binary systems. And ternary contribution term is marked with L_{CrFeNi}^L. This ternary term can be treated with the following formulation (eq. 2):

$$L_{CrFeNi}^L = x_{Cr}\,{}^0L_{CrFeNi} + x_{Fe}\,{}^1L_{CrFeNi} + x_{Ni}\,{}^2L_{CrFeNi} \quad (2)$$

In a similar way the calculation conducted for other substitutional solid solution phases, e.g., austenite, ferrite, etc. Additionally, a magnetic contribution, $\Delta^{mg}G$ must be added. Here, *mg* defines the magnetic free energy. By adding the carbon in second sublattice, when extending the system to quaternary Fe-Cr-Ni-C, a so-called interstitial solution model is implemented: $(Cr,Fe,Ni)_a(C,Va)_b$. The *a* and *b* represent the site ratios. Where *b* for the b.c.c. structure is b=3 and for the fcc structure b=1. The *Va* stands for vacancy.

Models with sublattices

A large group of intermetallic phases (s, μ, R etc.) are modeled using the sublattice model. A typical example is the brittle σ-(sigma) phase. Normally the recommendation for the description of the sigma phase is to use three sublattices with the site ratios 10:4:16. In some other assessments, site ratios 8:4:18 had also been used [7]. The model with three sublattices is described with the expression for one mole of formula units:

$(A,B,\ldots)_{a1}(K,L,\ldots)_{a2}(U,V,\ldots)_{a3}$

$$G_m = \sum_i\sum_j\sum_k y_i^{/}y_j^{//}y_k^{///}\,{}^0G_{i:j:k} +$$

$$+RT\left(\begin{array}{l} a_1\sum_i y_i^{/}\ln(y_i^{/}) + a_2\sum_j y_j^{//}\ln(y_j^{//}) + \\ a_3\sum_k y_k^{///}\ln(y_k^{///}) \end{array}\right) + {}^EG_m$$

Where: *I*, *II*, *III* represent the first, second and the third sublattice and *i, j, k* in our case study represent Fe, Cr and Ni respectively. ${}^EG_m$ represents excess Gibbs energy contribution. The important parameters to be optimized are those in the surface of reference, ${}^0G_{i:j:k}$. y^I, y^{II} and y^{III} represents site fractions on the first (commonly occupied with by f.c.c. elements), second (mainly b.c.c. elements) and the third sublattice (a mixture of all). If excess Gibbs energy is taken into account, then the calculation is done using the following formulation:

$$\begin{aligned} {}^EG_m = &\sum_i\sum_j\sum_k\sum_{l>i} y_i^{/}y_j^{//}y_k^{///}y_l^{/}L_{i,l:\mathrm{j:k}} + \\ &+\sum_i\sum_j\sum_k\sum_{l>i} y_i^{/}y_j^{//}y_k^{///}y_l^{//}L_{i:\mathrm{j,l:k}} + \\ &+\sum_i\sum_j\sum_k\sum_{l>k} y_i^{/}y_j^{//}y_k^{///}y_l^{///}L_{i:\mathrm{j:k,l}} + ... \end{aligned}$$

The parameters $L_{i,l:j:k}$ describe the mutual interaction of constituents *i* and *l* in the first sublattice, when the second and third sublattice is occupied with the constituents *j* and *k*, respectively:

$$L_{i,l:j:k} = \sum_i {}^iL_{i,l:j:k}(y_i^{/} - y_l^{/})^i$$

In the systems with more than three components the occupation on sublattices can be expanded by adding components as Co, Mo etc. [11] which are (typical) alloying elements for stainless steels. In this study the sigma phase is modeled using three sublattice model $(Cr,Fe,Ni)_{10}(Cr)_4(Cr,Fe,Ni)_{16}$. From formulae the mixing of constituents on the first and the third sublattice is seen.

3 Results

3.1 Differential scanning calorimetry

As relevant representatives of stainless steels the duplex and austenitic grades were selected. The specimens for differential scanning calorimetry

experiments (DSC) were taken from the hot-rolled steel plates of commercial origin. Their chemical compositions are given in Table 1.

Table 1. *Chemical composition of steels / wt.%*

Type	C	Si	Mn	Cr	Ni	Mo	N	Fe
Duplex SAF 2205	0.024	0.49	1.4	22.41	5.31	3.13	0.165	Balance
Austenitic AISI304LN	C	Cr	Ni	Mn	Cu	Si	N	Mo
	0.021	18.32	8.29	1.31	0.56	0.3	0.1	0.31
	Co	Fe						
	0.218	Balance						

The DSC experiments were performed using Netzsch-STA 449 C Jupiter apparatus up to 1550 °C. The measurements for austenitic stainless steel were performed using 10 K/min scan rate. On the other hand, 5 K/min scan rate was used in case of duplex stainless steel. The DSC experiments were conducted under static atmosphere of nitrogen of 99.999 vol.% purity. This was done to prevent any changes of local chemical composition of a bulk material due to oxidation or evaporation of elements, in particular, nitrogen. In both cases, an empty corundum crucible was used as reference. Because temperature derivate of the enthalpy versus temperature determines the DTA or DSC response of the particular Fe-based alloy (the delta function) [12], the calculation of heat capacity for both real alloy systems was done for easier interpretation of data.

Duplex stainless steel

Several endothermic peaks were identified on the DSC heating curve (Figure 1). This confirms the complexity of the melting sequence [13]. Normally, duplex stainless steels primarily solidify as ferrite (b.c.c.). When liquid is enriched with austenite-stabilizing elements it can rich the eutectic rim ($L \rightarrow \alpha + \gamma_1$) and an additional peak can be observed. The intensity of the "second" DSC peak depends on the intensity of segregation. Nevertheless, this reaction is also possible to determine when using different approaches of calculation of phase diagram: using complete chemical composition or using calculated nickel and chromium equivalent.

The solid state transformation is expected ($\alpha \rightarrow \gamma_2$) where austenite precipitates and, therefore, a matrix of ferrite and austenite is formed. The temperature of crossing from the one-phase ferrite region into two-phase region ($\alpha + \gamma_2$) depends on the equivalents of nickel and chromium ($Ni_{eq.}$ and Cr_{eq}). Approx. under 800 °C, the σ-sigma (tetragonal), χ-chi (b.c.c), Cr_xN_y (hexagonal) and secondary carbides like $M_{23}C_6$ (f.c.c) are expected to be stable. According to Pohl et al. [13]

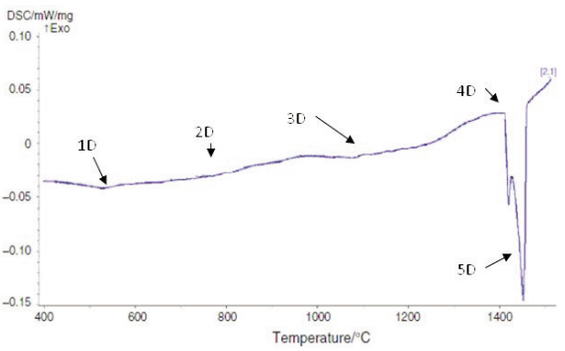

Figure 1. *Duplex stainless steel-SAF 2205; 5K/min*

the χ-phase is usually thermodynamically not stable when σ-phase is precipitating. The precipitation of σ-sigma phase is related to depletion of the neighboring ferrite in Cr and Mo and vice versa, enrichment in Ni. In this way ferrite becomes unstable and decomposes into γ_3 [14].

The measured DSC heating curve goes very well with the reported DTA measurements performed on similar duplex steel [15]. The first peak (1D) with onset at 448.5 °C and maximum 527 °C is related with the dissolving of precipitated α'-chromium-rich phase. Second endothermic peak (2D) with onset at 706 °C goes very well with the calculated Curie temperature 706 °C. Nevertheless, because this peak has no characteristic shape it is assumed that heat was mainly absorbed for the γ_3 transformation where σ-phase with other carbides and nitrides also dissolves. At temperature 967.4 °C disappearance of austenite take place following reaction $\gamma_2 \rightarrow \alpha$ (3D). Nevertheless, having segregated liquid present the DSC curve will show also the crossing of the three phase region ($\gamma + \alpha + L$), i.e. solidus (4D peak). Next thermal event, designated with 5D represents the melting of primarily solidified ferrite.

Austenitic stainless steel

The DSC heating curve was also characterized by several endothermic peaks (Figure 2). Thermal event at 797.9 °C (1A) represents the dissolving of carbides, sigma phase, and nitrides. Second endothermic reaction with onset at 1200 °C could be related to the $\gamma_2 \rightarrow \alpha$ transformation (2A). Next peak at 1426 °C (3A) represents solidus temperature (crossing of three phase ($\alpha + \gamma + L$) region). The last peak represents melting of primarily solidified ferrite (4A). According to Huang et al. [16] the solidification is with primary ferrite precipitation. The austenite precipitates with peritectic reaction. Normally, there is always a competition between peritectic/eutectic reaction.

3.2 THERMODYNAMIC CALCULATIONS

Thermodynamic calculations were performed

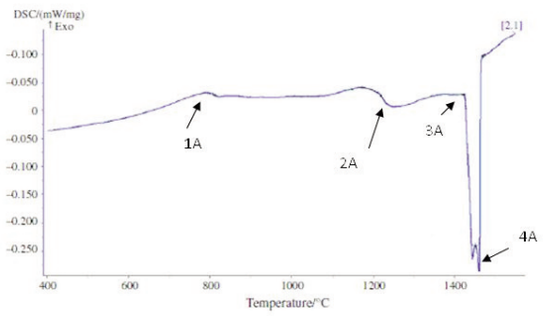

Figure 2. *DSC heating curve: austenitic stainless steel-AISI 304LN; 10 K/min*

using Thermo-Calc (TCW5) software and the new TCFE7 thermodynamic database for iron-based alloys. Relevant and reliable binary phase diagrams are the first step in understanding of ternary and multicomponent phase equilibria. Therefore, in Figure 3 the calculated binary phase diagrams obtained by CALPHAD method versus phase diagrams proposed by Massalski et al. are represented [20]. A relatively good agreement between calculated (Figs. 3a, c, e) and experimentally determined results (Figs. 3b, d, f) is clearly evident. Binary phase diagrams were calculated using database TCBIN. On the other hand, when using the database TCFE7, the calculated results for Fe-Ni phase diagram showed a rather high discrepancy on Ni-rich side. For further investigations of stainless steels three binary phase diagrams, i.e., Fe-Cr, Fe-Ni, Ni-Cr, are important for the ternary Fe-Cr-Ni system calculations.

Fe-Cr system

From Figures 3 a and 3b a chromium addition in iron restricts so called gamma loop closed between A4 (1394 °C) and A3 (912 °C). One intermetallic compound phase (FeCr) is observed, the sigma phase. The sigma phase exhibits certain range of homogeneity. The ferrite microstructure is observed also at room temperature. The precipitation of Cr-rich α' phase is somewhere between 370 °C and 540 °C and the α' is well-known because of so-called 475 °C embrittlement phenomenon [17].

Fe-Ni system

Two primary regions exist in this system, with α-ferrite with b.c.c. and g-austenite, f.c.c. crystal structure. There is peritectic reaction present with the next reaction: L + α→γ. Additional, in as-solidified alloys at higher nickel content $FeNi_3$ compound is expected, Figure 3 c,d. The peritectic reactions in Fe-Ni system was studied also by Nassar [18].

Ni-Cr system

There is eutectic reaction present with L→γ + δ. In the Massalski phase diagram [20] there is an obvious intermediate $CrNi_2$ phase (gamma'). In literature some assessments can be found where $CrNi_2$ is taken as a stochiometric compound [19]. The data in Figure 3 e are represented without the thermodynamic data of $CrNi_2$.

Fe-Ni-Cr system

It can be seen from Figure 4 that the solidification in Fe-Cr-Ni ternary system is possible in austenitic (A), austenitic-ferritic (AF) and ferritic (F) region. According to monovariant line in Fe-Ni-Cr ternary system the solidification can be completed with the eutectic reaction. According to [1] the peritectic reaction begins in the Fe-Ni system and changes to eutectic reaction before exiting the ternary field towards Cr-Ni system. By lowering the temperature a change in orientation appears for three phase region (L + α + gamma), see Figure 4 b. According to Fredriksson [21] the transition from peritectic to eutectic reaction in Fe-Cr-Ni system is at approx. 17.2 % Cr and 11.9 % Ni. According to Okane and Umeda [22] this can be at approx. 15 % Cr and 10 % Ni and according to Kundrat and Elliot [1] this is at 9.5 % Cr and 7 % Ni. However, at higher iron contents a peritectic reaction is expected. The peritectic reaction seems to be also possible in high-alloy steels because of segregation effects [23]. This is also assumed for austenitic 304 type of steel [23]. In the case of solidification if (FA) or (AF) mode is expected that one phase region of austenite will be reached after crossing two phase (δ + γ) region. The temperatures of crossing this two-phase region are highly dependent on the composition of steels and also on the cooling rates which affects the position of characteristic temperatures. A good agreement is obtained between calculated liquidus projection using TCFE7 and the one reported by Hillert and Qiu [2], see Figure 4 b.

4. Discussion

Real alloy systems – Duplex and austenitic stainless steels

For simplicity, the solidification paths of austenitic and duplex stainless steels may be studied using Fe-Cr-Ni ternary system, as already discussed before. In case of stainless steels there could be at least four different types of solidification paths regarding to the non-equilibrium or equilibrium states of cooling. The type of the solidification mechanism can be roughly estimated already by using chromium and nickel equivalent, Cr_{eq} and Ni_{eq}, respectively. There can be solidification in austenitic (A), austenitic-ferritic (AF), ferritic-austenitic (FA) and ferritic mode (F) [24]. Furthermore, the equilibrium solidification thermal effects of real and more complex alloy systems can also be represented with the calculated

heat capacity of duplex stainless steel using their complete chemical compositions (Table 1).

For the duplex stainless steel SAF 2205 the specific heat can be seen in Figure 5. In Figure 5a the

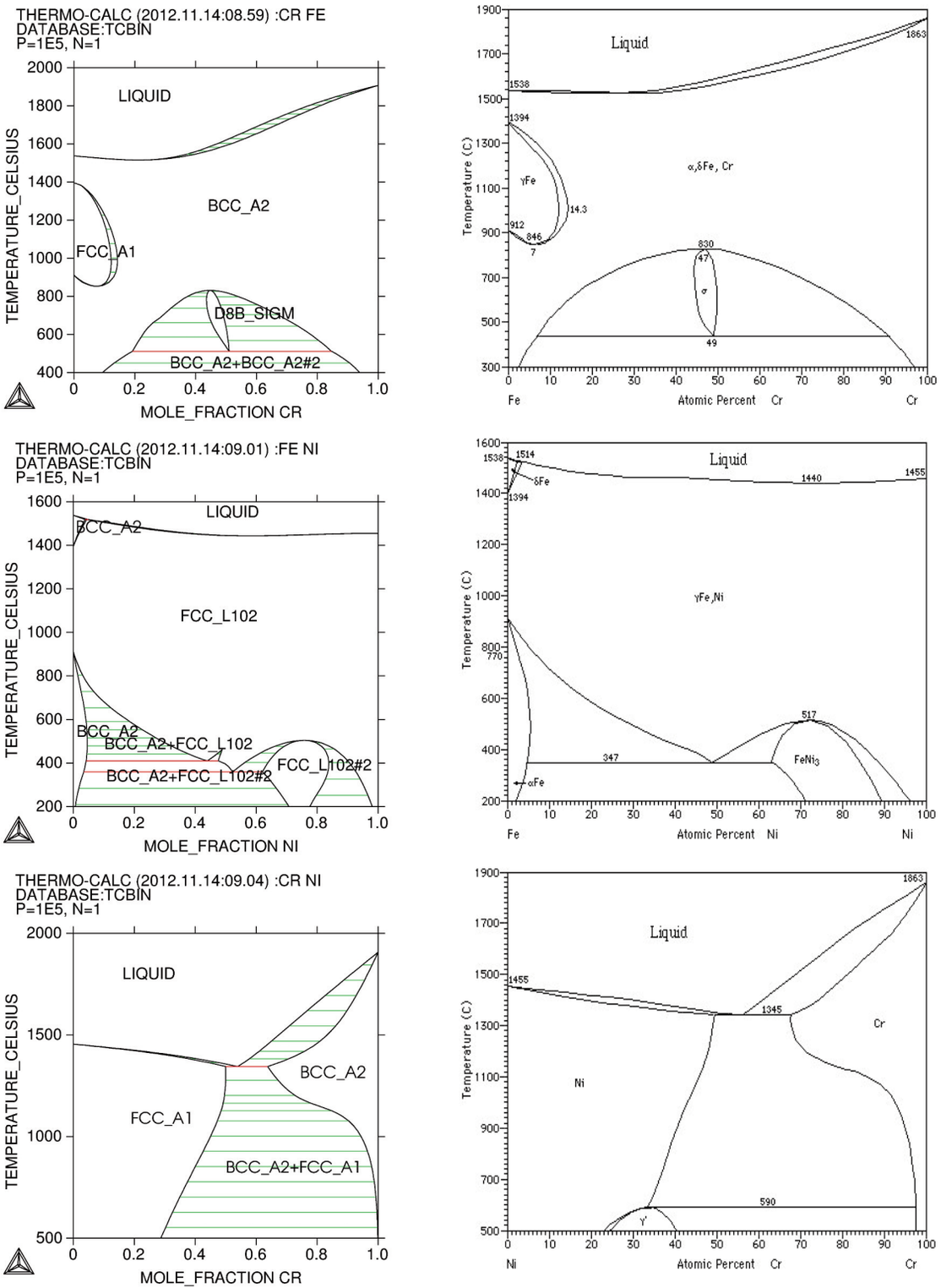

Figure 3. *(a, b) Cr-Fe, (c, d) Fe-Ni and (e, f) Ni-Cr system [20]*

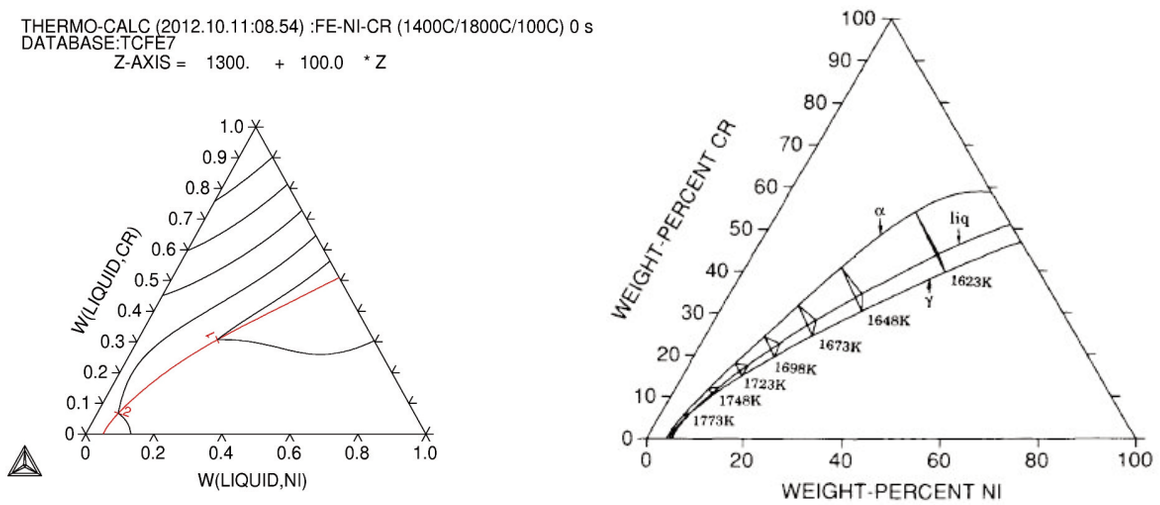

Figure 4. *The ternary phase diagram Fe-Ni-Cr: (a) Calculated using internal thermodynamic database of TCFE7 and (b) calculated three-phase equilibrium L + α + γ reported by Hillert and Qiu [2] All data for the calculations are referred to Standard Element Reference (SER).*

calculation is based on nickel and chromium equivalent and in Figure 5b the calculation takes into account the complete chemical composition.

In industrial environment, much estimation on solidification mechanism are performed based on calculations of relationship between chromium and nickel equivalents. In our previous work [25] some of the proposed sets of expressions for the Cr-equivalent and Ni-equivalent are summarized. It was shown that there are many models available for predicting the solidification mechanism of austenitic stainless steels. Using different sets of formulae the results can be very scattered. Also, the presence of alloying elements other than Cr and Ni limits the use of available Fe-Cr-Ni phase diagram for assessing the solidification sequence.

In the present case study on duplex stainless steel the calculated thermal effects are similar for both chemical compositions (partial and complete), see Figure 5 a, b. The solidification for both calculations proceeds in ferritic (F) mode. In the case of partial chemical composition(Cr_{eq} and Ni_{eq}), a small one-phase (ferritic) region exists where afterwards the second thermal effect is expected by solid-solid precipitation of austenite phase γ_2 from ferrite. No peritectic/eutectic reaction is predicted. Third effect is due to the formation of σ-sigma phase. Also here the crossing of the two-phase region ($\sigma + \gamma_3$) is visible. Last peak is related with the formation of α', the Cr-rich ferritic (b.c.c.) phase.

In the case of complete chemical composition the last liquid solidifies by crossing three phase region (L + α + γ) where f.c.c. austenite precipitates. Because this reaction takes a small part for the given

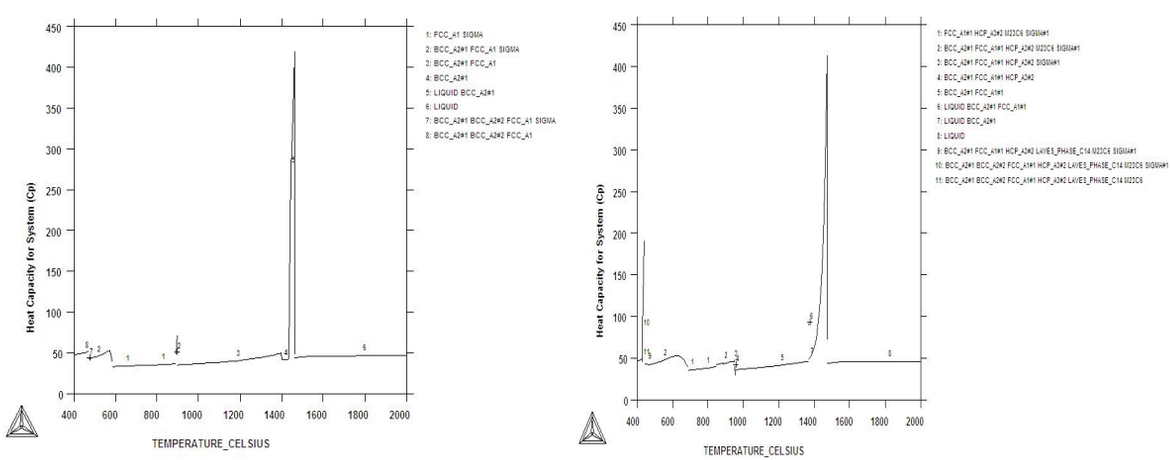

Figure 5. *Specific heat (Lever) for duplex– SAF 2205 in $Jmol^{-1}K^{-1}$; gas suspended: (a) calculation is based on nickel and chromium equivalent and (b) calculation using complete chemical composition.*

composition this was not visible through phase fraction-temperature in our previous study [26]. Therefore, the differences in the predicted solidification mode using the partial or the complete chemical composition may lead to the conclusion that the use of Cr_{eq} and Ni_{eq} in the solidification studies should be used only after critical assessment.

Taking into account the heat capacity calculations, these effects are intense and easily observed, see Figure 5 b. The type of reaction (peritectic/eutectic) depends on the orientation of the three-phase region ($L + \alpha + \gamma$). After solidus is reached, there is already a duplex structure present. At lower temperatures precipitates are formed like phase with h.c.p. crystallographic structure (assuming M_xN_y), σ-sigma and $M_{23}C_6$. According to calculations it seems that at approx. 840 °C, ferrite phase is no longer present (crossing the solvus line and entering in two-phase region ($\sigma + \gamma_3$)). But ferrite starts again precipitating at lower temperatures when entering back into the two-phase region of duplex microstructure.

In the present study, the solidification sequence of austenitic stainless steel using only its complete chemical composition (see Table 1) was calculated with representation of heat capacity as a function of temperature. The results are shown in Figure 6.

The calculated heat response presented in Figure 6 of AISI304 LN revealed the solidification with the primary formation of α-ferrite (with b.c.c. crystallographic structure). Additional vertical jump of heat capacity reveals that according to equilibrium solidification this proceeds in the three-phase region ($L + \alpha + \gamma$). The precipitated γ-phase from liquid has the f.c.c. crystallographic structure. Nevertheless, α-ferrite will slowly transform into austenite. Also here the presence of sigma phase is calculated at lower temperatures.

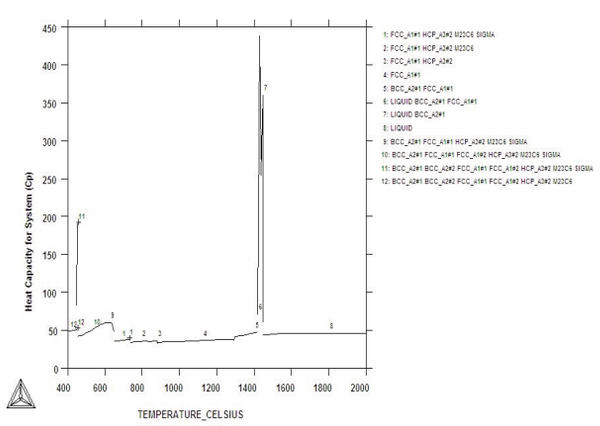

Figure 6. *Specific heat (Lever) for austenitic stainless steel - AISI304LN Joule per mol-K.*

5. Conclusions

Computational thermodynamics normally describes the equilibrium state of system under given conditions, and gives information of phase transitions important for many industrial processes.

For simplicity, the melting behavior as well as solidification paths of austenitic and duplex stainless steels may be studied using Fe-Cr-Ni ternary system.

Furthermore, the equilibrium solidification thermal effects can also be represented with the calculated heat capacity using their complete or partial chemical compositions. The use of Cr_{eq} and Ni_{eq} in the solidification studies should be used after critical assessment.

DSC heating curves for selected duplex and austenitic stainless steels revealed several endothermic peaks which confirm the complexity of the melting sequence in real alloy systems.

Regarding the calculated heat capacity diagrams for both stainless steels a relativelly good agreement was obtained between the thermodynamic calculations and experimental results, in spite of the complexity of both real alloy systems.

References

[1] D. M. Kundrat, J. F. Elliott, Metallurgical transactions A, 19 A (1988) p. 899-908

[2] M. Hillert, C. Qiu, Metallurgical Transactions A, 21 A, (1990) p. 1673-1680

[3] Y. Pan, C. Qiu, Transactions of NFsoc, 5 (2) (1995) p. 76-84

[4] M. Ceylan, V. Kuzucu, M. Aksoy, I. Aksoy, M. Kaplan, M. M. Yildirim, Journal of materials Processing Technology 69 (1997) p. 238-246

[5] J. Janovec, B. Šuštaršič, J. Medved, M. Jenko, MTAEC9, 37 (6) (2003) p. 307-312

[6] http://www.calphad.org/

[7] H. L. Lukas, S. G. Fries, B. Sundman, Computational Thermodynamics; The Calphad Method, Cambridge university press, New York, 2007, p.79-157

[8] V. Raghavan, D. P. Antia, Metallurgical and Materials transactions A, 25A, (1994) p. 2675-2681

[9] A. T. Dinsdale, CALPHAD 15 (4) (1991) p. 317-425

[10] O. Redlich, A. T. Kister, Ind. Eng. Chem., 40 (1948) p. 345-348

[11] http://www.thermocalc.com/res/pdfDBD/TCNI5_extended_info.pdf

[12] W. J. Boettinger, U. R. Kattner, K.-W. Moon, J. H. Perepezko, DTA and Heat-flux DSC Measurements of Alloy Melting and Freezing, NIST Recommendation Practice Guide, 2006, p.19

[13] M. Pohl, O. Storz, T. Glogowski, Materials characterization, 58 (2007) p. 65-71

[14] E. Erişir, U. Prahl, W. Bleck, 6th International Advanced Technologies Symposium (IATS11), 16-18 May, Elezig, Turkey, 2011, p. 471-474

[15] J. L. Beckers, P. Moureaux, M. Carton, A. M. Habraken, Phys. stat. sol. (a), 203 (15) (2006) p. 3651-3664

[16] F. Huang, X. Wang, J. Zhang, C. Ji, Y. Fang, Y. Yu, Journal of iron and steel research, International 15 (6) (2008) p. 78-82

[17] P. Hedström, Doctoral Thesis, Luleå University of Technology, Sweden 2007, p.6

[18] H. Nassar, Doctoral Thesis, KTH, Stockolm, Sweden 2009

[19] P. E. A. Turchi, L. Kaufman, Z. K. Liu, CALPHAD, 30 (1) (2006) p. 70-87

[20] T. B. Massalski, et al., Binary Alloy Phase Diagrams. 2 ed, ASM Int.: Materials Park, OH. 1990

[21] H. Fredriksson, Solidification and casting of metals, The metal Society, London 1979 p.131-138

[22] T. Okane, T. Umeda, ISIJ International, 38 (5) (1998) 5 p. 454-460

[23] V. Shankar, T. P. S. Gill, S. L. Mannan, S. Sundaresan, Frontiers in materials science (B. Ray, B. S. Rao) Bangalore: Universities Press, India 2005 p.359-382

[24] K. Rajasekhar, C. S. Harendranath, R. Raman, S.D. Kulkarni,. Mater, Charact. 38 (1997) p. 53-65

[25] D. S. Petrovič, G. Klančnik, M. Pirnat, J. Medved, J. Thermal. Anal. Calorim. 105 (1) (2011) p. 251-257

[26] D. S. Petrovič, M. Pirnat ,G. Klančnik, P. Mrvar, J. Medved, J.Therm. Anal. Calorim. 109 (3) (2012) p. 1185-1191